Fine Structure of the $2\,^3P$ and $3\,^3P$ States in Helium*

I. WIEDER† AND W. E. LAMB, JR.‡
Stanford University, Stanford, California
(Received April 2, 1957)

The $2\,^3P_2-2\,^3P_1$, $3\,^3P_1-3\,^3P_0$ and $3\,^3P_2-3\,^3P_1$ level separations in orthohelium are determined experimentally by extending previously developed microwave-optical techniques. Frequencies of 2291.72±0.36 Mc/sec, 8113.78±0.22 Mc/sec, and 658.55±0.15 Mc/sec, respectively, are found for the above level separations. These results are to be compared with previous optical measurements of 2295±21 Mc/sec for $2\,^3P_2-2\,^3P_1$, 7950±600 Mc/sec for $3\,^3P_1-3\,^3P_0$, and a microwave-optical determination of 658±1 Mc/sec for $3\,^3P_2-3\,^3P_1$.

I. INTRODUCTION

IN A recent paper[1] Lamb proposed a method for making microwave measurements of the fine structure of short-lived excited states of atoms, and presented pertinent calculations for the particular case of the $n\,^3P_J$ states of orthohelium. At the same time, Lamb and Maiman[2] used this method to obtain a value of 658±1 Mc/sec for the $3\,^3P_2-3\,^3P_1$ separation, and described the general apparatus which was utilized in obtaining their result.

This paper deals with the application of the method to other $n\,^3P_J$ fine-structure separations. In order to clarify the nature of the experimental difficulties a brief review of the method will be given. For a more detailed description reference is made to the previous papers in this series.[1,2]

Helium atoms in an external magnetic field are excited from the $1\,^1S_0$ state to $n\,^3P_J$ levels by electron bombardment. These atoms decay to the metastable $2\,^3S_1$ state in approximately 10^{-7} second, emitting optical radiation (see Fig. 1). The radiation pattern depends upon the populations of the various sublevels of the $n\,^3P_J$ states. If the excited atoms are subjected to an rf magnetic field of the proper frequency, the populations of two sublevels are modified (if they were originally unequal in population) and the optical radiation pattern is changed. Because of the presence of the external magnetic field, the various transitions occur at field-dependent frequencies. Thus, it is possible to search for an rf absorption by applying an rf magnetic field at a fixed frequency, varying the external magnetic field, and observing the intensity of optical radiation in a given direction. Standard modulation techniques are used and resonances are displayed on a recorder. The center of a resonance is located and a simultaneous observation of external magnetic field and frequency of applied rf is made. The theory of the Zeeman effect is then used to calculate the fine structure.

Lamb's calculations[1] included Zeeman effect, rf matrix elements, and expected change of polarization of optical radiation at rf saturation. The field dependence of transition frequencies is shown in Fig. 2, and the squared matrix elements and optical-radiation intensity changes are given in Table I.

II. EXPERIMENTAL VERIFICATION OF RELATIVE PREDICTED SIGNAL

In view of the discrepancy between the calculated and observed polarization[2] and the relatively weak signals expected from some of the resonances to be studied, it was desirable to first establish the reliability of the calculated relative signal of the various transitions. The theory could then be used in choosing one of the many possible transitions for each case of interest.

From Fig. 2 it is seen that the "π" transitions "9" through "14" are convenient from the standpoint of being observable at a fixed rf frequency in the working

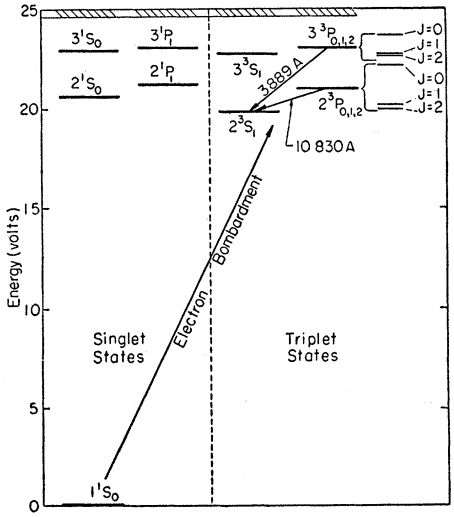

FIG. 1. Optical spectrum of helium. The triplet states are characterized by parallel electron spins and are produced by electron bombardment of helium. The $3\,^3P_J$ and $2\,^3P_J$ states decay in about 10^{-7} second to the metastable $2\,^3S_1$ state emitting optical radiation as shown.

* Research supported by the Office of Naval Research. This paper is based on a thesis submitted in July, 1956, by I. Wieder in partial fulfillment of the requirements for the degree of Doctor of Philosophy in Physics at Stanford University.

† Present address: Westinghouse Research Laboratories, Pittsburgh 35, Pennsylvania.

‡ Present address: Clarendon Laboratory, University of Oxford, Oxford, England.

[1] W. E. Lamb, Jr., Phys. Rev. **105**, 559 (1957). Referred to as Part I in the text.

[2] W. E. Lamb, Jr., and T. H. Maiman, Phys. Rev. **105**, 573 (1957). Referred to as Part II in the text.

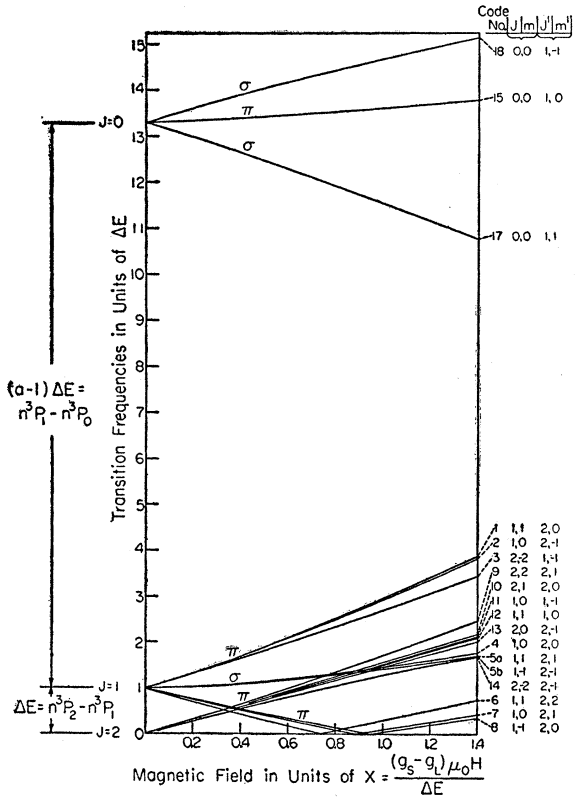

FIG. 2. The Zeeman effect for the $n\,^3P_J$ levels in helium. Enlarged plots of the lower part of this diagram were given in Figs. 10–11 of Part I. This plot was useful as a guide in searching for resonances, and is valid for all n if the ratio of the separations, $(a-1)$, is constant and the results are expressed in terms of the dimensionless variables x and y. The zero-field values, ΔE and $(a-1)\Delta E$, were taken from results of the optical experiments.

range of magnetic field. Furthermore, Table I shows that they all have large squared matrix elements and should therefore be observable at a (fixed) low level of rf amplitude. Finally, the experimental factors are readily held constant for all these transitions, thus providing a real test of the theoretically predicted linear relationship between the relative signal and the product $\Delta I_{\rm II}|V|^2$, for values of rf far below saturation.[1]

The $3\,^3P$ spectrometer previously described[2] was modified by changing the orientation of the rf magnetic field, and the above six transitions were detected. Figure 3 shows experimental recorder traces taken far below rf saturation, while Fig. 4 is a plot of peak-to-peak signal *versus* $\Delta I_{\rm II}|V|^2$, using values of $\Delta I_{\rm II}$ and $|V|^2$ from Table I. Since every sublevel of the $J=2$ and $J=1$ levels is involved in these transitions, a good basis is established for the use of the theory to predict relative signals.

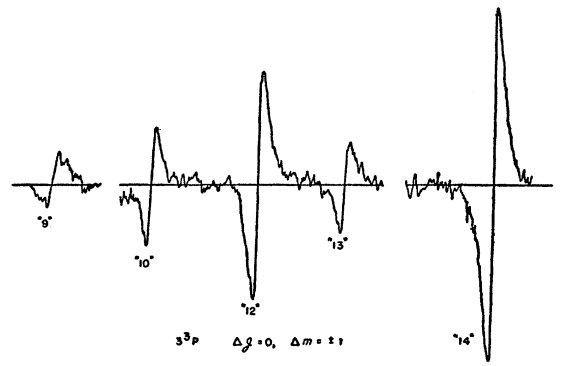

FIG. 3. Recorder traces of transitions "9" through "14" taken at about 900 Mc/sec.

III. DETECTION OF A $3\,^3P_1-3\,^3P_0$ TRANSITION

1. Choice of Transition

An examination of Fig. 2 reveals three possible transitions, "15," "17," and "18," which can be used to determine the larger separation of the $3\,^3P$ fine structure. As Table I shows, "17" has the largest intensity by a factor of about 5 and the lowest squared matrix element by a factor of about 3. Since this latter factor can be overcome in principle by working near saturation, transition "17" was selected. The Zeeman behavior of this transition in the working range of external magnetic field indicates that a (perpendicular) rf magnetic field in the range 6700–7400 Mc/sec is required (see Fig. 2).

TABLE I. Intensity changes, $\Delta I_{\rm II}$, and squared matrix elements, $|V|^2$, at various magnetic fields. The working range of magnetic field (300–600 gauss) corresponds to a range in x of 0.2–0.35 for the $2\,^3P$ case and 0.6–1.2 for the $3\,^3P$ case.

Transition code No.	$x=0.2$		$x=0.3$		$x=0.6$		$x=0.9$		$x=1.2$	
	$\Delta I_{\rm II}$	$\lvert V\rvert^2$	$\Delta I_{\rm II}$	$\lvert V\rvert^2$	$\Delta I_{\rm II}$	$\lvert V\rvert^2$	$\Delta I_{\rm II}$	$\lvert V\rvert^2$	$\Delta I_{\rm II}$	$\lvert V\rvert^2$
1	0.01	0.07	0.00	0.09	0.10	0.14	0.35	0.18	0.61	0.20
2	1.38	0.19	1.55	0.25	1.88	0.38	1.99	0.47	1.96	0.52
3	0.65	0.40	0.51	0.51	0.22	0.78	0.11	1.01	0.05	1.20
4	1.66	0.32	1.56	0.31	1.10	0.24	0.68	0.18	0.38	0.14
5a, b	0.15	0.24	0.66	0.23	2.12	0.18	3.58	0.14	4.70	0.11
6	1.42	0.13	1.66	0.08	2.29	0.01	2.79	0.01	3.12	0.03
7	0.60	0.07	0.45	0.04	0.12	0.01	0.01	0.00	0.01	0.01
8	0.26	0.02	0.33	0.14	0.50	0.00	0.56	0.00	0.56	0.00
9	0.65	2.30	0.51	2.43	0.22	2.50	0.11	2.50	0.05	2.50
10	0.26	3.42	0.33	3.42	0.50	3.33	0.56	3.22	0.56	3.15
11	0.60	1.10	0.45	1.18	0.12	1.28	0.01	1.39	0.01	1.45
12	1.38	1.08	1.55	1.15	1.88	1.24	1.99	1.35	1.96	1.40
13	0.01	3.30	0.00	3.20	0.10	2.96	0.35	2.74	0.61	2.55
14	1.42	2.15	1.66	2.00	2.29	1.72	2.79	1.49	3.12	1.35
15	0.45	0.66	0.39	0.65	0.27	0.62	0.16	0.58	0.10	0.55
17	0.30	0.33	0.39	0.31	0.72	0.27	1.02	0.24	1.25	0.21
18	0.05	0.34	0.00	0.35	0.08	0.36	0.18	0.37	0.20	0.38

2. Expected Signal-to-Noise Ratio

For the microwave spectrometer utilized in this experiment, the signal-to-noise ratio is limited by shot noise from the photocathode.[2] A useful form of a formula for signal-to-noise ratio (assuming rf saturation) can be written

$$S/N \propto \Delta I_{\rm II}\left(\frac{\tau I P \sigma_n E}{1+i_E/i_{\rm He}}\right)^{\frac{1}{2}}, \qquad (1)$$

where τ is the band-width limiting time constant of the detection system, I is helium tube excitation current, P is the helium pressure, σ_n is the excitation cross section for the n triplet levels, E is the quantum photoefficiency of the photocathode, i_{He} is the photocurrent due to the appropriate helium transition and i_E is the extraneous photocurrent. On the basis of the observed value of S/N for transition "5," a first estimate of expected S/N for "17" was made by assuming rf saturation and no changes in experimental parameters. Under these conditions the S/N should vary as ΔI_{II}. From the observed value of 50/1 for "5" (see Part II) an expected S/N of 12/1 was calculated for "17." In practice, a factor of 3 in S/N was lost due to a decrease in light-collecting efficiency imposed by the small size of the cavity needed for this transition, so that the expected S/N is only about 4/1 at rf saturation.

Using the formula for half-saturation derived in Part I, Sec. X,

$$H_1^2 \sim 1/|V|^2, \tag{2}$$

and substituting $|V|^2$ from Table I, one finds that 2 gauss of rf magnetic field are required to reach half saturation. An estimated Q_L of 7500 was needed to reach this value if readily available power sources were to be utilized.

3. Design of Excitation Tube

The excitation tube differed from the one reported previously[2] in that the section which was to go inside the cavity was changed to quartz because Nonex was found to be lossy at the required frequency. Other changes included the incorporation of a nonmagnetic barium getter, and a Pyrex bulb about 0.02 inch thick and a few square inches in surface area for admission of helium to the tube by diffusion.

4. Design of Cavity

To provide the necessary rf amplitude, a reflection-type half-wavelength resonant cavity with an inductive iris coupler was constructed (see Fig. 5). The basic structure was a section of "J"-band wave guide with a plate silver-soldered to one end. Holes (a) for the excitation tube were placed so that the tube would be as near as possible to the maximum rf magnetic field and as far as possible out of electric fields which would disturb the beam. Radiation chokes (b) were used wherever possible. The observation hole (g) and Polaroid rotating mechanism (h) were mounted in a direction perpendicular to the tube axis and as close to the tube as possible without interacting with the cavity fields. A good match was obtained by keeping the diaphragm (c) removable and adjusting the iris (d) until a standing-wave ratio of about 1 was observed with the tube in place. Dielectric tuning was accomplished by using a quartz rod (e) which could be moved continuously between two extreme positions corresponding to a range of 6900–7600 Mc/sec. The cavity was monitored by an electric-field probe (f). The loaded Q was observed to be about 3000 with the excitation tube in place.

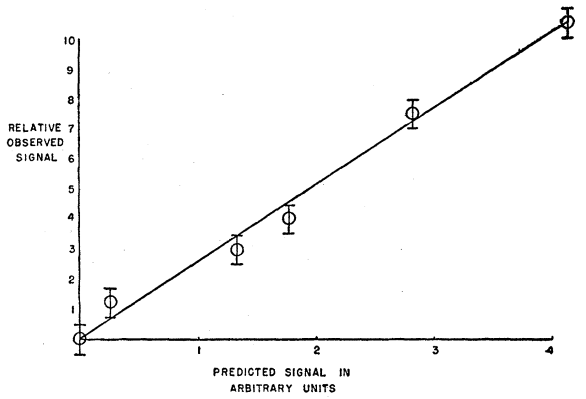

FIG. 4. Plot of peak-to-peak observed signal against relative signal predicted by the theory of Part I.

5. Tube Filling and Resonance Detection

Since the cavity did not have the desired Q, it was expected that it would be necessary to increase the excitation electron current and the helium pressure in order to observe a resonance. Owing to the difficulty in designing high-perveance electron guns, the decision was made to try an increased pressure alone. On the other hand, there are upper limits of helium pressure (and electron current) imposed by possible "self-reversal"[3] of the optical light, electron-beam stability, and pressure broadening. Also, the possibility of a

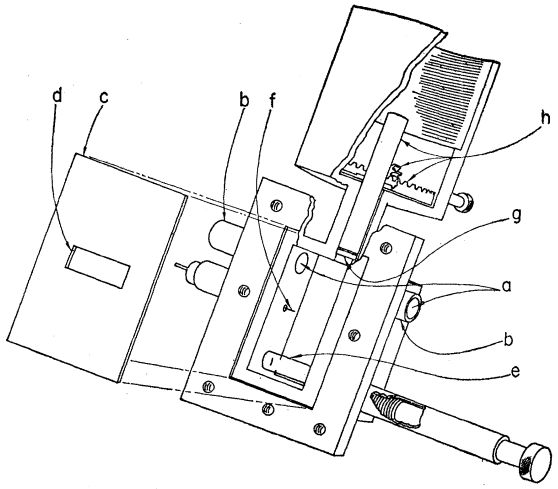

FIG. 5. Schematic diagram of tunable high-Q cavity for the high-frequency $3\,^3P$ transition.

[3] Brochard, Chabbal, Chantrel, and Jacquinot, J. phys. radium **13**, 433 (1952). The results quoted in Part I for the optical measurements using this paper as reference were in error for the $2\,^3P_2-2\,^3P_1$ separation. The correct value is 2295±21 Mc/sec.

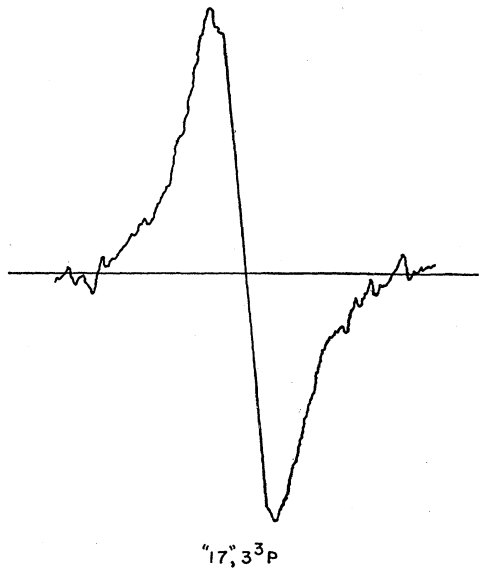

FIG. 6. Transition "17"$-3\,^3P$ observed at 7000 Mc/sec and 480 gauss. The peak-to-peak width is about 1.8 gauss.

variable pressure was ruled out by previous failures associated with kinetic systems.[2] For these reasons it was necessary to monitor the tube continuously while the helium was being admitted. The plan was to let in only enough helium to attain a reasonable S/N. Unfortunately, helium diffusion through glass is not completely understood, although enough empirical data had been accumulated for us to expect a considerable delay before the result of an exposure to helium would manifest itself in the tube. The presence of helium gas in the tube would first be noticed by the appearance of 3889 A optical radiation, and, ultimately, (it was hoped) by a resonance.

With the tube in place in the spectrometer, the Pyrex bulb was exposed to helium at 1 atmosphere in a series of short exposures followed by long periods of observation. After a total exposure of 25 minutes, the pressure reached an estimated 30 microns of helium and a resonance of considerable S/N was observed (see Fig. 6).

IV. DETECTION OF A $2\,^3P_2-2\,^3P_1$ TRANSITION

1. Selection of Transition

A measurement of the $2\,^3P$ fine structure is possible in principle with the same basic apparatus used for $3\,^3P$. The main changes involved are differences in the frequency of applied rf magnetic field and detected optical-decay light.

An atom in the $2\,^3P$ excited state decays in approximately 10^{-7} second to the $2\,^3S$ metastable state with an associated emission of infrared radiation at 10 830 A. This lifetime is about the same as the $3\,^3P$ lifetime so that no significant change of line width is to be expected. The 10 830-A radiation to be detected, however, has considerably less energy per quantum than 3889 A radiation from $3\,^3P$, and its detection proved to be a serious problem.

In order to estimate the probability of success of the proposed measurement, it was first noted that calculations of matrix elements, optical intensity changes, and Zeeman effect are independent of the total quantum number of the ^3P level if the ratio of separations, $(a-1)$, is about the same for the 2 cases, (see Fig. 2), and the results are expressed as functions of the dimensionless magnetic-field variable x. An inspection of Fig. 2 and Table I reveals three possible choices of transitions, "2," "6," and "4," that reduce to the desired ΔE in zero external field and have reasonable intensities and matrix elements in the accessible magnetic field ($x=0.2-x=0.35$). A power source was not readily available in the frequency range required for "2," so the choice was restricted to "4" or "6." Transition "6" was chosen since it occurs in a more convenient frequency range than "4" and has the further advantage of being similar to "2" of the $3\,^3P$ pattern in that both resonances require a perpendicular rf magnetic field in the vicinity of 1500 Mc/sec. The only significant difference in the detection of the two resonances is in the wavelength of the detected optical radiation. Thus, estimates of expected S/N could be obtained by direct comparison of "2"$-3\,^3P$, and "6"$-2\,^3P$, and since "2" is a readily accessible resonance the apparatus could be improved until the observed S/N of "2" reached a value which predicted a reasonable S/N for "6."

2. Selection of Infrared Detector

A survey of existing detectors with response at 10 830 A revealed that a photosurface with an $S-1$ response had the highest inherent S/N ratio, because of the fact that its primary noise source is photoelectron shot noise. Furthermore, it was clear that a photomultiplier with its essentially noiseless gain was superior to a phototube and electronic amplifier since the Johnson noise at the input resistor of the amplifier exceeded the anticipated shot noise (for a modulation method) at that point.

Several DuMont K1430 infrared photomultipliers were obtained and checked for sensitivity at 10 830 A, and the best one selected. A comparison of the quantum photoefficiencies of this tube and the R.C.A. 6199 photomultiplier used for the $3\,^3P$ resonances showed the K1430 to be only 1/2500 as efficient at 10 830 A as the 6199 at 3889 A.

3. Expected S/N Ratio

By means of Eq. (1) it is possible to estimate the ratio of the S/N ratios of "2"$-3\,^3P$ and "6"$-2\,^3P$ under the following conditions:

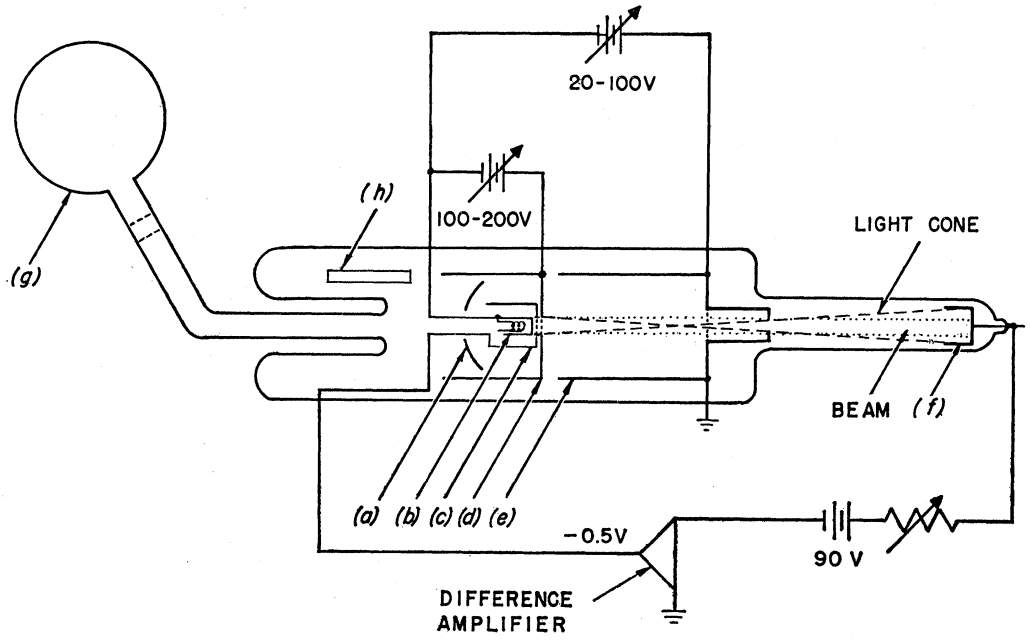

FIG. 7. Schematic diagram of excitation tube and current-regulating power supply used to detect infrared resonance. The tube operated at 500 μa at a pressure of about 20 microns. The over-all tube length is about six inches.

(a) $i_E=0$,

(b) same degree of rf saturation attainable on both resonances,

(c) same pressure and current in excitation tube, and

(d) no self-reversal in either case.

The ratio becomes

$$\frac{S/N(\text{“}6\text{”}-2\,^3P)}{S/N(\text{“}2\text{”}-3\,^3P)}=\frac{(\Delta I_{11})_6}{(\Delta I_{11})_2}\left\{\left(\frac{E'}{E''}\right)\left(\frac{\tau'}{\tau''}\right)\left(\frac{\sigma_2}{\sigma_3}\right)\right\}^{\frac{1}{2}}. \quad (3)$$

The values for ΔI_{11} can be obtained from Table I, the ratio E'/E'' was measured to be 1/2500, the maximum reasonable value for τ'/τ'' is about 25 and the ratio σ_2/σ_3 has been measured[4] to be about 3. Substituting these values and arbitrarily assuming a desired S/N for “6”$-2\,^3P$ of 5/1, one calculates a S/N of 40/1 for “2”$-3\,^3P$.

Of the conditions for Eq. (3) listed above, only (a) and (b) are difficult to satisfy and will be considered below.

4. Cathode Light and Dark Current

The bulk of the extraneous photocurrent i_E is produced by scattered light from the hot cathode, and the remainder is dark current. These effects are both much larger in red-sensitive tubes than in blue for two reasons: (a) Stray light from the cathode is peaked in the infrared. (b) Photosurfaces in red-sensitive tubes must have low work functions and hence high dark current. This means that i_E is larger for $2\,^3P$ resonances and reduces the expected S/N calculated above. The quantity i_E/i_{He} was measured in the infrared using the existing excitation tubes and was found to be about 100. In order to attain the proposed S/N for “6”$-2\,^3P$, it would now be necessary to gain a factor of 10 in the calculated S/N for “2”$-3\,^3P$. However, this could be obtained only by introducing a factor of 100 in the product IP; and even if the excitation tube worked at these high pressures and currents, there would be an increased chance for self-reversal to set in. Furthermore, self-reversal is more likely in the infrared than in the blue. Thus, it was clear that the cathode light had to be eliminated in order to detect a resonance.

Attempts to use 10 830 A interference filters were frustrated, as all those available diminished both beam and cathode light in a ratio which would result in a very small increase in S/N. Moreover, the decreased intensity of beam light made it necessary to operate the photomultiplier at an increased gain. This introduced instabilities and noise not present in the usual operation. Various optical schemes were tried, but failed for the same reasons. It became apparent that a system which discriminated completely against cathode light and did not affect beam light would be needed.

5. Excitation Tube

A new excitation tube was designed and is illustrated in Fig. 7. The cathode (b) was moved back to a point where electrode geometry confined the cone of direct light. The collector electrode (f) and final accelerator electrode (e) were blackened on the inside, as were the baffles (a) which were placed behind the filament. The

[4] Bates, Fundaminsky, Leech, and Massey, Trans. Roy. Soc. (London) A243, 117 (1950).

control electrode (c) and first accelerator (d) were not blackened to eliminate the possibility of heat liberating gases from the blackening material and the cathode becoming "poisoned." A Pyrex diffusion bulb (g) for helium and a nonmagnetic getter (h) were mounted as before.

After processing in the usual way, the tube was placed in the spectrometer, but due to the increased length of electron path, the magnetic field was found to be inadequate for confining the beam. Helium was then allowed to diffuse through the Pyrex bulb in the hope that helium ions would neutralize the space charge which was spreading the beam. Unfortunately, it was not possible to monitor a resonance during this process, so helium diffusion was continued until the combined effects of space-charge neutralization and magnetic field were sufficient to confine the beam.

With the beam on, the cathode light was found to have been attenuated to a point where any further decrease would result in, at most, a factor of $\sqrt{2}$ in S/N. Dark current was virtually eliminated by cooling the photomultiplier with solid CO_2. With the condition that $i_E=0$ essentially fulfilled, it was now necessary to investigate the possibility of rf saturation of both resonances.

6. rf Cavity

The transitions involved both require a perpendicular rf magnetic field of about 1500 Mc/sec. Their squared matrix elements are 0.12 for "6"$-2\,^3P$ and 0.47 for "2"$-3\,^3P$ in their respective accessible regions, and according to Eq. (2) and Table I they need 2.5 and 1.4 gauss respectively for half saturation.

Figure 8 shows the cavity that was designed in an attempt to provide 2.5 gauss of transverse rf magnetic field. The cavity was excited by a variable-capacity probe (a) and tuned by varying the position of rod (b). A separate match was required for each position of the tuner and was obtained by varying the position of the coupler. A probe (e) was used for monitoring the cavity, and the entire assembly was placed in a piece of wave guide for shielding. Holes (f) for the excitation tube were placed in the cavity and box so that the interaction space was in a region of maximum rf magnetic field (c) and far away from strong electric fields which were confined to the gap (d).

An estimate of the power required for 2.5 gauss of rf magnetic field at the measured Q_L of 300 revealed

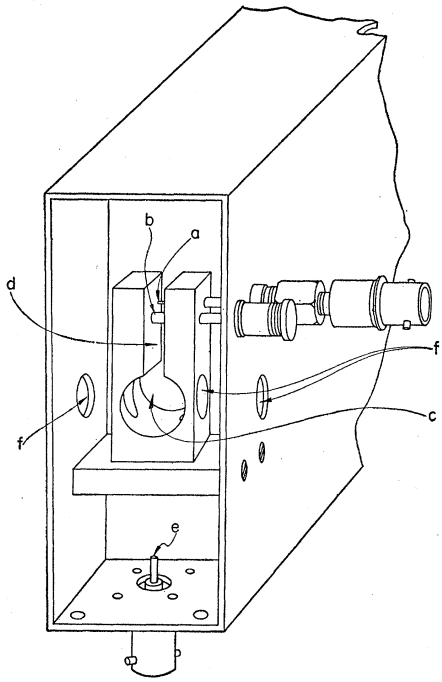

FIG. 8. Schematic diagram of tunable cavity used to generate 2 gauss of perpendicular rf magnetic field at 1500 Mc/sec.

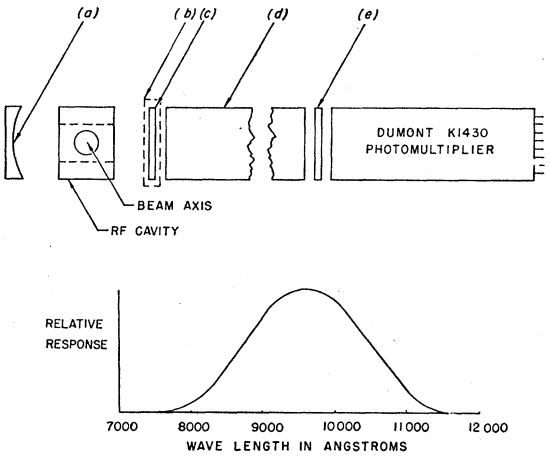

FIG. 9. Schematic diagram of infrared optical system and its relative spectral response curve.

that 10 watts would be needed. This power was available, but caused electrical breakdown to occur at the tuner and coupler. This limited the rf magnetic field to about 2 gauss, and slightly reduced the expected S/N of the resonances.

7. Optical System

It was necessary to place the photomultiplier some distance away from the external magnetic field in order to prevent its disturbance by stray fields. In the 3889 A case a Lucite light pipe was used to guide the decay light to the photomultiplier. Lucite was found to be absorbent at 10 830 A and was replaced by a hollow silvered tube. Figure 9 shows this tube (*d*) in relation to the cavity and excitation tube. A silvered mirror (*a*) was placed behind the cavity and served to increase the effective solid angle of the light detector. An infrared transmitting Polaroid (*c*) was placed in the rotating

assembly (b), and a Corning 2540 filter (e) was put in front of the photomultiplier.

The spectral response of the combination of an $S-1$ surface and 2540 filter is also shown in Fig. 9. A check of expected intensities of other optical transitions in this range of wavelength revealed that their contribution was negligible in comparison to the 10 830 A radiation.

8. Detection of Resonances

The blue optical system was installed, with the sine-wave modulation amplitude set at twice the expected resonance width to maximize[5] S/N. The transition "2"$-3\,^3P$ was found to have a S/N of about 60/1 with a time constant of 6 seconds. From the above considerations it seemed that the infrared resonance should now be detectable, with a S/N of 7/1, so the infrared optical system was installed, the time constant was increased to 150 seconds, and the magnetic-field sweep rate was slowed down accordingly. A search of the expected region revealed an infrared resonance as predicted (see Fig. 10).

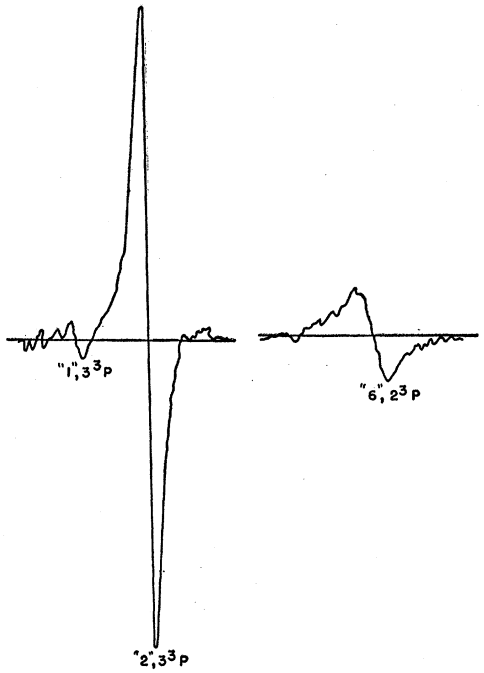

FIG. 10. Recorder traces of "2"$-3\,^3P$ and "6"$-2\,^3P$.

9. Remarks on $2\,^3P_1-2\,^3P_0$ Separation

A high-power source at 1 cm was not readily available so that a direct determination of the larger $2\,^3P$ separation was not possible at the time these measurements were made.

[5] R. Beringer and J. Castle, Jr., Phys. Rev. 78, 581 (1950).

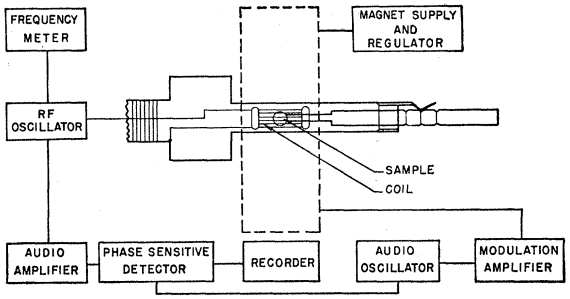

FIG. 11. Schematic diagram of magnetic-field measuring apparatus.

It is possible, in principle, to determine $2\,^3P_1-2\,^3P_0$ by observing certain transitions of the smaller separation. This comes about due to a mixing of states in the external field so that the $m=0$ levels are affected by the larger separation. A careful measurement of the Zeeman behavior of "3," for example, could yield such information. In practice, however, the effect is so small in the range of accessible magnetic field that it would be unnoticed even if a S/N of 100 could be attained.

V. MEASUREMENT OF RESONANCES

1. Magnetic Field Measurement

It is necessary to observe both the external magnetic field and transition frequency for calculation of the fine structure from Zeeman theory. The magnetic field was determined by use of an absorption-type proton resonance apparatus. Figure 11 shows a coil and proton sample which can be substituted for the excitation tube. The oscillator is a conventional Q multiplication feedback circuit, and is fed into the same circuitry as the output of the photomultiplier for resonance detection and display. Provisions were made to map a region $\frac{1}{2}$ in. long and $\frac{1}{8}$ in. in diameter by having the sample movable inside the fixed coil. The sample consists of about 0.05 cc of a 0.03-molar paramagnetic-ion solution which gives sufficient relaxation to cause line widths to be limited by a modulation of 0.1 gauss amplitude. Resonances of about 20/1 S/N ratio were detected over the range 300–600 gauss.

The proton resonant frequency ν_p is related to the magnetic field H by the formula

$$\nu_p=(\gamma/2\pi)H. \tag{4}$$

The value used for the constant was 4.25787 kc/gauss, any correction for sample shape and paramagnetism being negligible for this work. The resonant frequency ν_p was measured to 0.001%. Since the constant $(\gamma/2\pi)$ has been measured to 1 part in 50 000, the frequency uncertainty did not introduce a significant error in the magnetic field determination.

Owing to the modulation method of resonance detection, the observed resonance is roughly in the form of the derivative of a Lorentzian line shape. Since the

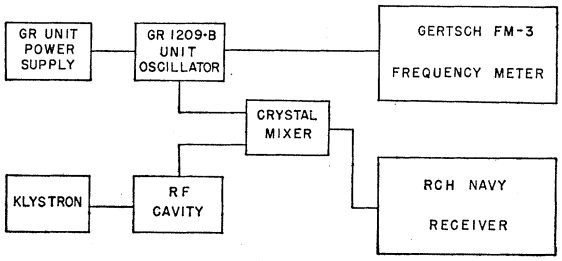

FIG. 12. Schematic diagram of frequency-measuring apparatus.

center of such a line is a point of zero slope, it is coincident with the point formed by the intersection of the derivative curve and the base line.

It would have been desirable to take data by locating the center of the resonance and simultaneously observing the applied frequency and external magnetic field. In practice it was impossible to have the proton coil and excitation tube positioned simultaneously. This difficulty was overcome by monitoring the current through the magnet. This was accomplished to a high degree of accuracy by observing the voltage drop across a series reference resistor with a Leeds and Northrup potentiometer. The potential was then calibrated with proton resonances taken before and after the helium resonances. Since the magnet is an air-core type, the potential V is related to the field by a linear equation of the form

$$H=cV+d. \tag{5}$$

By observing proton resonances at two points in the vicinity of the resonant field, the constants c and d were determined and the potential calibration accomplished.

In practice, the helium resonance was found and displayed on the recorder with the automatic field sweep to check for asymmetries and to define the base line. Then the center of the resonance was located and a frequency measurement and potentiometer reading taken simultaneously. This potentiometer reading was later used to determine the magnetic field as mentioned above.

2. Frequency Measurement

This was accomplished by mixing radiation from the rf source with a harmonic of a G.R. (1209-B) oscillator in a crystal mixer and listening to the beat note at about 2 Mc/sec in a receiver with good image rejection. The fundamental frequency of the G.R. oscillator was simultaneously monitored by a Gertsch FM/3 frequency meter (see Fig. 12). The accuracy of these measurements was about 0.02 Mc/sec and was limited by the breadth of the beat note heard on the receiver.

TABLE II. Deviation of the magnetic field from H_c, the central value, averaged over the interaction region.

Transition	$(\delta H)_{Av}$ (gauss)	H_c (gauss)
"5", $3\,^3P_2-3\,^3P_1$	+0.06	520
"2", $3\,^3P_2-3\,^3P_1$	+0.15	350–400
"17", $3\,^3P_1-3\,^3P_0$	+0.085	350–500
"6", $2\,^3P_2-2\,^3P_1$	+0.15	350–400

3. Results of Measurements

The results of applying the above method to various detected transitions are tabulated and analyzed in the next section.

VI. CALCULATION OF THE FINE STRUCTURE

1. Sources of Error

a. Measurement of H.—The measurement of the magnetic field at a given point in the spectrometer is accurate to at least 0.02 gauss in the working region. The uncertainty is due to that of the constant $(\gamma/2\pi)$ and the difference in the induced diamagnetic fields resulting from the excitation tube and proton apparatus.

b. Measurement of ν_0.—The measurement of transition frequency, ν_0, is accurate to at least 0.03 Mc/sec for a given determination in all cases. This uncertainty is reduced to approximately 0.01 Mc/sec by using the average of several observations for the quoted experimental value.

c. Constants.—The Zeeman calculation depends upon several constants. The values[6] used are tabulated below:

$\mu_0=0.92731\pm0.00002\times10^{-20}$ erg/gauss,

$h=6.62517\pm0.00023\times10^{-27}$ erg-sec,

$g_S=2.0022908$ (accurate to about one part in 50 000).

The remaining constant g_L is subject to a center-of-mass correction[7] and was taken to be

$$g_L=1-(m_e/m_{\mathrm{He}})=0.99986,$$

where m_e and m_{He} are the masses of the electron and helium nucleus respectively. Since the above formula was derived for a hydrogen atom, it is subject to a correction[8] due to interaction of the two orbital electrons. This correction is estimated to be less than one part in 10^5 of g_L so that all the above constants are accurate to at least one part in 30 000 and do not introduce significant errors in the results.

d. Unsymmetrical line shape.—Deviations from symmetry due to nonlinear Zeeman effect, variation of matrix elements and ΔI_{11} with magnetic field, and magnetic field inhomogeneity can cause small shifts of the resonance. These effects have been estimated and contribute negligible amounts to the total uncertainty.

e. S/N limitations.—The location of the center of a resonance is uncertain by an amount which can be roughly expressed as

$$\Delta H=\frac{(\text{peak to peak width in gauss})}{(S/N)}. \tag{6}$$

[6] Cohen, DuMond, Layton, and Rollet, Revs. Modern Phys. **27**, 363 (1955).
[7] W. E. Lamb, Jr., Phys. Rev. **85**, 259 (1952).
[8] M. Phillips, Phys. Rev. **76**, 183 (1949).

This quantity is about 0.1 gauss for a single determination in a typical case, and, being a random error, can be virtually eliminated by taking many measurements.

f. Field inhomogeneity.—The magnetic field was inhomogeneous by about 0.1 gauss over the interaction region. This broadened the resonances slightly and shifted their peaks by an amount that is readily calculable in principle. If the resonance signal is of the form $S(H-H_0)$ where H_0 is the resonant field, it can easily be shown that a negligible error is made by assuming a uniform field of $(H)_{Av}$ in the interaction region and using that field to calculate the fine structure.

In computing $(H)_{Av}$, it is necessary to correct for rf magnetic field inhomogeneity (negligible in this experiment) and variation of intensity changes and detector solid angle with θ, the angle between the axis of quantization and the detector. The procedure is as follows: first, proton resonances are used to map the field. Because of the finite size of the sample, only three independent points are taken along the axis in the interaction region. Using these three points, one determines an average detector angle θ for each location and estimates the total solid angle Ω of the detector. The effective rf-induced change of z-polarized optical radiation is then computed for each average angle by using[9,1]

$$\Delta I_{11}(\theta)=\Delta I_{11}\sin^2\theta+\Delta I_{\perp}\cos^2\theta, \tag{7}$$

and

$$\Delta I_{11}=-2\Delta I_{\perp}. \tag{8}$$

The measured values of H at each point are then multiplied by a number proportional to the product $\Delta I_{11}\Omega$ and a weighted average taken. The difference between $(H)_{Av}$ and the central-field value is thus determined for a given magnetic field and is denoted by $(\delta H)_{Av}$.

Because of severe signal-to-noise limitations on $2\,^3P_2-2\,^3P_1$, it was not possible in that case to utilize an experimental configuration which would lend itself to a direct estimate of $(\delta H)_{Av}$. An indirect determination was made by utilizing the fact that $(\delta H)_{Av}$ was the same for "2"$-3\,^3P$ and "6"$-2\,^3P$ and is discussed in Part C of the next section. The results of these determinations of $(\delta H)_{Av}$ are shown in Table II.

2. Reduction of Data

a. Transition "5."—$(3\,^3P_2-3\,^3P_1)$. The Zeeman formula for this transition is obtained by combining formulas for $W(2,\pm1)$ and $W(1,\pm1)$. The result is given in Eq. (11) of Part I. Denoting E_1-E_2 by ΔE, the observed transition frequency by ν_0, and expressing ΔE and ν_0 in units of Mc/sec one can solve for ΔE, obtaining

$$\Delta E=\left(\nu_0^2-\frac{(g_S-g_L)^2\mu_0^2H^2}{h^2}\right)^{\frac{1}{2}}\text{ Mc/sec.} \tag{9}$$

[9] J. A. Smit, Physica **2**, 104 (1935).

TABLE III. Results of calculations of $3\,^3P_2-3\,^3P_1$ using transition "5."

Obs ν_0 (Mc/sec)	Obs H_c (gauss)	$(H)_{Av}$ (gauss)	ΔE (Mc/sec)	δ (Mc/sec)	Wt
983.443	520.47	520.53	658.60	+0.05	10
983.405	520.50	520.56	658.50	−0.04	10
983.323	520.39	520.45	658.55	0.00	6
983.126	520.22	520.28	658.52	−0.03	10
983.623	520.66	520.72	658.57	+0.02	10
983.462	520.53	520.59	658.53	−0.02	10
983.439	520.49	520.55	658.56	+0.01	10

Weighted average = 658.55 Mc/sec

The results of applying this formula to the data are shown in Table III. Although the internal consistency is high, the quoted result is uncertain by a somewhat larger amount due to possible systematic errors. An estimated upper limit of the combined sources of error can be made by summing the absolute values of the calculated effect on the zero-field splitting due to all of the sources of error discussed in the previous section. The separation is therefore taken to be

$$3\,^3P_1-3\,^3P_0=658.55\pm0.15\text{ Mc/sec.}$$

b. Transition "17."—$(3\,^3P_1-3\,^3P_0)$. The Zeeman behavior of this transition is obtained by combining the formulas for $W(0,0)$ and $W(1,1)$ from Part I. If the levels are defined as

$$E_2=0,\quad E_1=\Delta E,\quad E_0=a\Delta E,$$

then the desired zero-field splitting becomes $(a-1)\Delta E$. Substituting these values into Eqs. (11) and (13) of Part I and introducing the dimensionless variables $w(j,m)=W(j,m)/\Delta E$, one can solve for $(a-1)$, obtaining

$$(a-1)=w(0,0)-\frac{\frac{2}{3}x^2w(0,0)}{w(0,0)^2-w(0,0)-\frac{1}{3}x^2}-1, \tag{10}$$

where x is defined as $(g_S-g_L)\mu_0H$ and $w(0,0)$ is calculated from

$$w(0,0)=w_{\text{obs}}+\frac{1}{2}\left(\frac{g_S+g_L}{g_S-g_L}\right)x+\tfrac{1}{2}(1+x^2)^{\frac{1}{2}}+\tfrac{1}{2}, \tag{11}$$

TABLE IV. Results of calculations of $3\,^3P_1-3\,^3P_0$ using transition "17."

Obs ν_0 (Mc/sec)	Obs H_c (gauss)	$(H)_{Av}$ (gauss)	$(a-1)\Delta E$ (Mc/sec)	δ (Mc/sec)	Wt
7182.25	405.55	405.63	8113.84	+0.06	6
7056.30	457.20	457.28	8113.74	−0.04	5
7003.00	478.98	479.07	8113.73	−0.05	5
7149.20	419.13	419.21	8113.80	+0.02	6
6936.50	506.15	506.24	8113.81	+0.03	6
6930.88	508.42	508.51	8113.76	−0.02	12
7301.10	356.40	356.48	8113.74	−0.04	12
7301.90	356.10	356.18	8113.82	+0.04	8
6965.30	494.40	494.48	8113.75	−0.03	6

Weighted average = 8113.78 Mc/sec

TABLE V. Determination of $(\delta H)_{Av}$ for the microwave-optical configuration used for "6"$-2\,^3P$ and "2"$-3\,^3P$.

Obs ν_0 (Mc/sec)	Obs H_c (gauss)	ΔE (H_c) (Mc/sec)	$(H)_{Av}$ calc (gauss)	$(\delta H)_{Av}$	Wt
1559.59	348.66	659.16	348.82	+0.16	8
1555.56	347.28	659.22	347.46	+0.18	4
1654.27	380.50	659.01	380.62	+0.12	11
1693.26	393.44	659.12	393.59	+0.15	14
			$(\delta H)_{Av}=+0.15$ gauss		

where w_{obs} is defined as the observed transition frequency ν_0 in units of ΔE. The results of applying these formulas to the data are shown in Table IV. An estimate of the upper limit of the uncertainty is made as before. The separation is taken to be

$$3\,^3P_1-3\,^3P_0=8113.78\pm0.22 \text{ Mc/sec.}$$

c. Transition "2."—($3\,^3P_2-3\,^3P_1$). The Zeeman behavior of this transition is obtained as before, Eqs. (14) and (11) of Part I being combined in this case. It is not convenient to solve for ΔE explicitly, so the formula is left in the form

$$w_{obs}=\frac{1}{2}\left[1+\tfrac{4}{3}x^2\left(1-\frac{2w(1,0)}{a-w(1,0)}\right)\right]^{\frac{1}{2}}+\frac{1}{2}\left(\frac{g_S+g_L}{g_S-g_L}\right)x+\tfrac{1}{2}(1+x^2)^{\frac{1}{2}}. \quad (12)$$

The value for $w(1,0)$ is obtained by iteration using the experimental value for a. Then the above equation is iterated and the process repeated for several assumed $(H)_{Av}$ until a value of $\Delta E=658.55$ Mc/sec (implicit in x) in the above equation is consistent with w_{obs}. Thus $(\delta H)_{Av}$ is determined for the microwave-optical configuration used in this and the "6"$-2\,^3P$ case. The results appear in Table V.

d. Transition "6."—($2\,^3P_2-2\,^3P_1$). In this case, the Zeeman behavior is obtained by combining Eqs. (9) and (11) of Part I. It is here convenient to solve for ΔE explicitly, obtaining

$$\Delta E=\frac{h^2\nu_0^2+h\nu_0(g_S+g_L)\mu_0H+\mu_0^2H^2g_Sg_L}{h\nu_0+\frac{1}{2}(g_S+g_L)\mu_0H} \text{ Mc/sec.} \quad (13)$$

TABLE VI. Results of calculations of $2\,^3P_2-2\,^3P_1$ using transition "6."

Obs ν_0 (Mc/sec)	Obs H_c (gauss)	$(H)_{Av}$ (gauss)	ΔE (Mc/sec)	δ (Mc/sec)	Wt
1611.16	335.12	335.27	2291.68	−0.04	1
1605.03	338.32	338.47	2291.83	+0.11	1
1609.18	336.15	336.30	2291.72	0.00	1
1609.24	335.96	336.11	2291.41	−0.31	1
1611.07	335.18	335.33	2291.71	−0.01	1
1611.72	334.94	335.09	2291.89	+0.17	1
1527.58	378.01	378.16	2291.80	+0.08	1
		Weighted average = 2291.72 Mc/sec			

The results of applying this formula to the data are shown in Table VI. An estimate of the upper limit of the uncertainty is made as before and one obtains

$$2\,^3P_2-2\,^3P_1=2291.72\pm0.36 \text{ Mc/sec.}$$

These results are much more precise than existing data and should be of use in theoretical work on helium fine structure. A comparison with previous results appears below:

Separation	Previous measurements	This paper
$3\,^3P_2-3\,^3P_1$	658±1 Mc/sec	658.55±0.15 Mc/sec
$3\,^3P_1-3\,^3P_0$	7950±600 Mc/sec	8113.78±0.22 Mc/sec
$2\,^3P_2-2\,^3P_1$	2295±21 Mc/sec	2291.72±0.36 Mc/sec

VII. ACKNOWLEDGMENTS

The authors would like to thank Dr. Lynn R. Sarles, Jack Maling, and Professor E. T. Jaynes for information used in designing various parts of the apparatus. Thanks are also due James F. Lee for his painstaking construction of excitation tubes and Mel Goodwin, Burton Stuart, and Leonard Manning for their precision machine work. The authors would also like to thank Lois J. Wieder for the numerical calculations of the fine structure.